UNIVERSITY OF COPENHAGEN
FACULTY OF SCIENCE

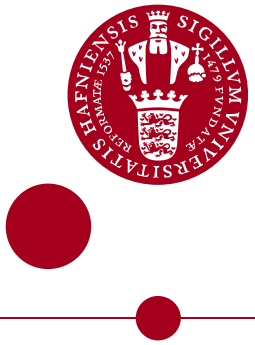

Bachelor Thesis

Numerical Simulations of Superconducting Qubits

Siri Stenstrup Hjermind

Advisor: Morten Kjaergaard

Submitted: January 17, 2025

This thesis has been submitted to the The Faculty of Science, University of Copenhagen

Abstract

Superconducting quantum computing is a rapidly advancing field with the potential to solve complex problems that are beyond the capabilities of classical computers. This thesis provides a comprehensive introduction to superconducting circuits, with a focus on their physical properties and numerical simulations. The study begins with an exploration of a circuit consisting of an inductor and a capacitor (LC circuit), which is formally equivalent to a quantum harmonic oscillator (QHO). In the quantum regime, the LC circuit exhibits discrete harmonic energy levels. A system can be used as a qubit when a computational subspace with only two energy states can be defined. This two-level system is achieved by introducing anharmonicity into the circuit, a task made possible by the Josephson junction, a nonlinear element. As a result, qubits can be constructed from circuits consisting of a Josephson junction and a capacitor (JC circuits). The numerical framework for simulating quantum systems is discussed, with a focus on implementing operators as discrete matrices. Simulations demonstrate the importance of the cutoff parameter in ensuring accurate eigenenergies and wavefunctions in numerical simulations. The relationship between wavefunction delocalization and qubit sensitivity to charge noise across different E_J/E_C regimes is also examined. In the small energy ratio regime, the wavefunction is highly localized, while in the large energy ratio regime, it becomes increasingly delocalized, reflecting reduced sensitivity to charge noise. As E_J increases, the potential profile of the JC circuit transitions toward a harmonic potential, gradually resembling the behavior of the LC circuit, an thus the anharmonicity decreases. Finally, the flux-tunable transmon, constructed using a SQUID (two Josephson junctions in parallel), is investigated. This design enables the ability to control the qubit "in situ" by adjusting the external flux, emphasizing its advantages in quantum computation.

Contents

Appendices

I. Introduction

Quantum Computing: A New Frontier

Quantum computing is a rapidly growing and exciting field. Some of its applications include cryptography [4] and computational speedup [12]. Unlike a classical computer, which stores information in bits. A quantum computer stores information in quantum bits (qubits). These qubits are governed by the laws of quantum mechanics, allowing phenomena like superposition and entanglement. [8]

Superconducting Quantum Computers

Superconducting material give rise to complex and exotic physics, only certain aspects are relevant for quantum computation. A superconductor is a material that, below its critical temperature T_C, allows dissipationless current flow. In the superconducting regime, the electrons in the metal form pairs known as Cooper pairs. These Cooper pairs share a common superconducting phase, denoted ϕ. The behavior of the superconductor can be described using the Ginzburg-Landau wavefunction:

$$\psi_{\mathrm{GL}}(\mathbf{r}) = |\psi(\mathbf{r})|e^{i\phi(\mathbf{r})} \tag{1}$$

One of the properties of superconductors is flux quantization, stating that the flux through a superconducting loop must be quantized, $\sum \Phi = k\Phi_0$. Where $\Phi_0 = h/2e$ is the unit of quantization and k is an integer.

Superconducting qubits are created from lumped element circuits and are macroscopic in size, as they are fabricated lithographically onto wafers. These systems lie in between microscopic particles, governed by quantum mechanics, and macroscopic objects, described by classical mechanics. They are referred to as mesoscopic systems. Essentially, this means that we have a macroscopic system that, when cooled down, exhibits behavior partially governed by quantum physics. [1, 13, 11]

Scope and Objectives of Thesis

This thesis serves as an introduction to superconducting circuits and their numerical implementation. In Section II, we explore the superconducting LC circuit with its harmonic potential, before moving on to discussing the anharmonic potential in JC circuits, introduced in Section III. Section IV. discusses the numerical framework used to simulate quantum systems. These simulation are presented in Section V. The thesis is rounded off in Section VI, where further applications and perspectives are discussed.

II. Superconducting LC-circuits

Classical Hamiltonian Description of the LC Circuit

The LC circuit is an electrical circuit consisting of an inductor and a capacitor (see Fig. 1 for the lumped-element model). The Hamiltonian of the LC circuit is derived using *Lagrangian-to-Hamiltonian transformation*, which is thoroughly described in [5]. The first step is to decide on which of the generalized coordinates, Φ (flux) or Q (charge), should represent the circuit elements in the Hamiltonian, i.e. picking a basis. For this derivation, the flux basis is chosen. See Appendix B for a derivation in the charge basis. The flux is a time integral of the voltage in the circuit.

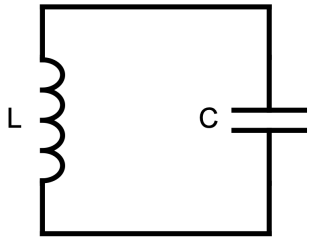

Figure 1: Lumped-element model of a circuit consisting of a capacitor and an inductor

$$\Phi(t) = \int_{-\infty}^{t} V(t')dt' \tag{2}$$

The Lagrangian is constructed from the kinetic and the potential energy. It can be useful to think of the generalized coordinates as one being momentum-like and one being position-like. Thus the electric energy in the capacitor and the magnetic energy in the inductor, can simply be thought of as the kinetic and the potential energy. The basis choice determines which of the general coordinates are position-like or momentum-like. For this derivation, since the flux is picked to represent the circuit elements, flux is analogous to the position coordinate and charge serves as the conjugate momentum. The electric energy stored in the capacitor thus represents the kinetic energy, while the magnetic energy in the inductor represents the potential energy. The instantaneous and time dependent energy in each element is:

$$E(t) = \int_{-\infty}^{t} V(t')I(t')dt' \tag{3}$$

By combining Eq. 2 and Eq. 3, along with the constitutive relations $I = C\frac{dV}{dt}$ for a capacitor and $V = L\frac{dI}{dt}$ for an inductor, we can derive expressions for the kinetic and potential energy.

$$\mathcal{T}_C = \frac{C}{2}\dot{\Phi}^2 \quad \text{and} \quad \mathcal{U}_L = \frac{1}{2L}\Phi^2 \tag{4}$$

See the complete derivation of the energy terms in Appendix A.

The Lagrangian is defined as the difference between the kinetic energy and the potential energy.

$$\mathcal{L} = \mathcal{T}_C - \mathcal{U}_L = \frac{C}{2}\dot{\Phi}^2 - \frac{1}{2L}\Phi^2 \tag{5}$$

The transition from Lagrangian to Hamiltonian requires a change in the variables from $(x, \dot{x}, t)$ to (x, p, t). The procedure of switching variables in this matter is done using a *Legendre transformation*. The canonical momentum is the following.

$$Q = \frac{\partial \mathcal{L}}{\partial \dot{\Phi}} \tag{6}$$

The Hamiltonian is obtained through the Legendre transformation.

$$H = Q\dot{\Phi} - \mathcal{L} = \frac{Q^2}{2C} + \frac{\Phi^2}{2L} = \frac{1}{2}LI^2 + \frac{1}{2}CV^2 \tag{7}$$

At this point, it's worthwhile to take a moment to reflect on our result. When the mass and resonant frequency are expressed using the capicatance and inductance, $m = C$ and $\omega = 1/\sqrt{LC}$, and we recall that the charge is position-like and the flux is momentum-like, we obtain the Hamiltonian for the harmonic oscillator, $H = p^2/(2m) + m\omega^2 x^2/2$. [9]

Quantizing the LC Circuit

The Hamiltonian we derived is purely classical and the generalized coordinates flux and charge satisfies the Poission brackets, confirming their canonical nature.

$$\{\Phi, Q\} = \frac{\partial \Phi}{\partial \Phi}\frac{\partial Q}{\partial Q} - \frac{\partial Q}{\partial \Phi}\frac{\partial \Phi}{\partial Q} = 1 \tag{8}$$

In quantum mechanics, canonical quantization promotes classical coordinates to operators that satisfy commutation relations derived from their Poisson brackets. Thus:

$$\Phi \to \hat{\Phi} \quad \text{and} \quad Q \to \hat{Q} \tag{9}$$

The commutation relation between the operators is:

$$[\hat{\Phi}, \hat{Q}] = \hat{\Phi}\hat{Q} - \hat{Q}\hat{\Phi} = i\hbar \tag{10}$$

This result should be recognizable as $[\hat{x}, \hat{p}] = i\hbar$ (see Appendix C).

In superconducting circuits, so-called reduced variables are often defined, as they simplify the mathematical description by transforming physical quantities into dimensionless forms. These variables include the reduced flux, $\phi \equiv 2\pi\Phi/\Phi_0$, and the reduced charge,

$n = Q/2e$. Here, Φ_0, is the superconducting magnetic flux quantum and can be found using $\Phi_0 = h/2e$, the constant represents the smallest "packet" of magnetic flux that can exist in a superconducting loop. The reduced flux, ϕ, is the superconducting phase introduced in the context of Ginzburg-Landau theory. It is 2π-periodic and it relates to the magnetic flux in the superconducting circuit. The reduced charge, n, is a measure for the amount of Cooper pairs existing in the circuit, as total charge, Q, is divided by the charge of two electrons ($2e$). Both of the reduced variables are only valid within the superconducting regime. The quantum mechanical Hamiltonian for the LC circuit expressed with reduced variables is therefore:

$$H = 4E_C\hat{n}^2 + \frac{1}{2}E_L\hat{\phi}^2 \tag{11}$$

Where the charging energy is $E_C = e^2/(2C)$ and the inductive energy is $E_L = (\Phi_0/(2\pi))^2/L$. The charging energy, E_C, describes the cost of adding a Cooper pair to the capacitor, while the inductive energy, E_L, characterizes energy stored in the magnetic field of the inductor. Together, they determine the harmonic dynamics of the circuit. [9]

Analysis of the LC circuit

By quantizing the classical Hamiltonian of the LC circuit, we arrive at a system that is formally equivalent to the quantum harmonic oscillator (QHO). This similarity to the QHO allows the use of its established solutions. These involve solving the time-independent Schrödinger equation.

$$-\frac{\hbar^2}{2m}\frac{d^2\psi}{dx^2} + V\psi = E\psi \tag{12}$$

Using the potential of a QHO, $V(x) = \frac{1}{2}m\omega^2x^2$ and $p = -i\hbar\frac{d}{dx}$ the Hamiltonian is obtained.

$$\frac{1}{2m}[\hat{p}^2 + (m\omega\hat{x})^2]\psi = E\psi \Rightarrow \hat{H} = \frac{1}{2m}[\hat{p}^2 + (m\omega\hat{x})^2] \tag{13}$$

Now, an algebraic method to solve this eigenvalue equation is to define the ladder operators, the creation, $\hat{a}_+$, and annihilation operator, $\hat{a}_-$ [1].

$$\hat{a}_\pm = \frac{1}{\sqrt{2\hbar m\omega}}(\mp i\hat{p} + m\omega\hat{x}) \tag{14}$$

The product of the two operators are:

$$\hat{a}_\pm\hat{a}_\mp = \frac{1}{2\hbar m\omega}(\mp i\hat{p} + m\omega\hat{x})(\pm i\hat{p} + m\omega\hat{x}) = \frac{1}{2\hbar m\omega}(\hat{p}^2 + (m\omega\hat{x})) \pm \frac{i}{2\hbar}[\hat{x}, \hat{p}] \tag{15}$$

[1] The ladder operators are also known as the raising and lowering operator and they're also denoted by $\hat{a}^\dagger$ and $\hat{a}$ respectively.

Using the canonical commutation relation between the operators $\hat{x}$ and $\hat{p}$. We can express the Hamiltonian using ladder operators.

$$\hat{a}_{\pm}\hat{a}_{\mp} = \frac{1}{2\hbar m\omega}(\hat{p} + (m\omega\hat{x})^2) \mp \frac{1}{2} \tag{16}$$

$$= \frac{1}{\hbar\omega}\hat{H} \mp \frac{1}{2} \tag{17}$$

$$\Rightarrow \hat{H} = \hbar\omega(\hat{a}_{\pm}\hat{a}_{\mp} \pm \frac{1}{2}) \tag{18}$$

Representing the Hamiltonian using ladder operators is known as the second quantization formalism. [2]

Any quantum mechanical system has a lower bound to its quantized energy levels known as the ground state energy. This means that when an annihilation operator is applied to the ground state energy, the result is just zero, $\hat{a}_-\psi_0 = 0$. This fact can be used to derive the ground state energy of the QHO, $\psi_0 = (\frac{m\omega}{\pi\hbar})^{\frac{1}{4}} e^{-\frac{m\omega}{\pi\hbar}x^2}$ (see Appendix D for a full derivation). The ground state energy can thus be found using Eq. 13, $E_0 = \frac{1}{2}\hbar\omega$. Successive states, $|n\rangle$, are obtained by applying $(\hat{a}_+)^n$, which leads to equally spaced energy levels.

$$E_n = (n + \frac{1}{2})\hbar\omega \tag{19}$$

[3]

III. Superconducting Qubits

A system can be used as a qubit when we are able to define a computational subspace consisting of only two energy states. Transitions between these two states, referred to as quantum gates, form the building blocks of quantum operations, while a specific sequence of gates constitutes an algorithm. Many gate operations depend on the frequency selectivity, thus a harmonic energy spectrum does not make a good qubit, as it is very difficult to confine the dynamics to just two levels, meaning leakage of the qubit subspace is a permanent threat. Therefore we can mimic a two level system by creating a system with anharmonic energy level spacing. We can calculate the qubit frequency $\omega_{01} = \frac{1}{\hbar}(E_1 - E_0)$, and then we will drive all of the transitions with that specific frequency. The anharmonicity of the quantum system is defined as:

$$\alpha = \hbar(\omega_{12} - \omega_{01}) = E_2 - E_1 - (E_1 - E_2) \tag{20}$$

[9, 11]

[2] Second quantization is also called the occupation number representation. This name might be a little more intuitive as the number operator is defined as: $\hat{n} = \hat{a}_+\hat{a}_-$.

Josephson Junction

Thus the key to making a qubit, is a circuit element that introduces anharmonincity in the energy-level spacing. This can be achieved by utilizing the nonlinearity of the so-called Josephson junction. There are different types of Josephson junctions, in this thesis I will always refer to the SIS-junction. The junction is made up of two superconducting islands with a small insulating gap in between, the gap between the superconducting islands is so small that it gives rise to quantum tunneling, this is a quantum mechanical phenomenon where particles pass through a potential energy barrier, which is classically forbidden.

The Josephson Junction is governed by the following constitutive relations:

$$I = I_C \sin(\phi) \quad \text{and} \quad V = \frac{\hbar}{2e}\frac{d\phi}{dt} \tag{21}$$

Here, ϕ represents the phase difference $\phi_2 - \phi_1$, where ϕ_1 and ϕ_2 are the superconducting phases on the first and second superconducting islands, and I_C is the critical current. When $I < I_C$, the current through the junction is dissipationless, i.e., a supercurrent, which is known as the dc Josephson effect. It is important to note that when the phase difference, ϕ, is constant, the voltage drop across the junction is zero, yet there is still a current due to the dissipationless supercurrent. It is the sine dependence of the current that is responsible for the anharmonic energy level spacing. [9, 3, 11, 1]

Cooper Pair Box

The Cooper pair box (CPB) is a qubit design consisting of two circuit elements: a capacitor and a Josephson junction. This design is also known as the JC circuit. The Hamiltonian is derived using the constitutive relations for the Josephson junction (Eq. 21).

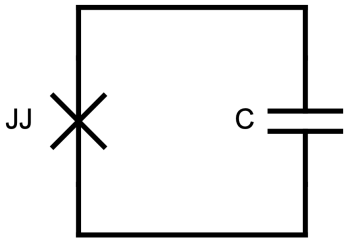

Figure 2: Lumped-element model of a circuit consisting of a capacitor and an Josephson Junction

$$\hat{H} = 4E_C\hat{n}^2 - E_J\cos(\hat{\phi}) \tag{22}$$

Here, $\hat{n}$ represents the Cooper pair number difference between the two superconducting islands, and $\hat{\phi}$ is the phase difference across the Josephson junction. The charging energy is given by $E_C = e^2/(2C_\Sigma)$, where $C_\Sigma = C_S + C_J$ is the total capacitance, including the shunt capacitance (C_S) and the Josephson capacitance (C_J). The Josephson energy is $E_J = I_C\Phi_0/(2\pi)$, where I_C is the critical current and Φ_0 is the

magnetic flux quantum.

In a superconducting circuit, charge pollution from other parts of the circuit can affect the system. To account for this, an environmental offset charge is introduced in the Hamiltonian.

$$\hat{H} = 4E_C(\hat{n} + n_{\text{offset}})^2 - E_J \cos(\hat{\phi}) \tag{23}$$

Here, n_{offset} represents the offset charge. This parameter is continuous because the influence of a pollution charge decreases with its distance from the system.

For a CPB, $E_C \approx E_J$. These energies can be adjusted during the qubit's topological design and fabrication process. The ratio between the Josephson energy and the charging energy determines key characteristics of the qubit, such as charge dispersion and anharmonicity. The charge dispersion is a description of the variation of energy levels with respect to the enviromental offset charge. Thus the charge dispersion also determines the charge sensitivity of the CPB. The CPB has a rather large charge dispersion meaning the qubit frequency will change in response to charge fluctuations. An approach to avoid this problem is to eliminate the linear noise sensitivity by operating the qubit at optimal working points, for the CPB this point is at $\frac{\Phi_0}{2}$. This approach is known as *sweet spot operation*.

These results are found from the analytical solution of the Hamiltonian for the JC circuit (Eq. 22). This Hamiltonian, when expressed in the phase basis, takes the form of Mathieu's differential equation and can therefore be solved using the so-called Mathieu functions. The process of solving this Hamiltonian analytically is beyond the scope of this thesis.[7, 10, 9]

The Transmon Qubit

Increasing the E_J/E_C ratio results in an exponential reduction in the charge dispersion while the anharmonicity only decreases algebraically with the slow power law. The gain in charge-noise insensitivity, achieved by increasing the E_J/E_C ratio, is thus paid for by the loss in anharmonicity. This principle was utilized by a new qubit design, called the transmon qubit, that came out in 2007. The transmon qubit consists of the same circuit elements as the CPB, and thus has the same Hamiltonian. It is designed to operate in a regime of a significally raised E_J/E_C ratio. This is known as the transmon regime.

$$E_J/E_C \geq 50 \tag{24}$$

In this regime, the charge dispersion vanishes for the lowest energy levels, resulting in a constant qubit frequency given by $\omega_{01} \approx \sqrt{8E_J E_C}/\hbar$. This frequency is known as the *Josephson plasma frequency*. The Josephson plasma frequency and the transmon frequency in the limit $(E_J/E_C)^{-1} \ll 1$, can be determined considering perturbation theory. Perturbation theory is a systematic procedure for obtaining approximate solutions to the perturbed problem by building on the known exact solutions to the unperturbed case. Expanding the potential of the transmon for small ϕ: $-E_J\cos(\hat{\phi}) \approx -E_J + E_J\hat{\phi}^2/2 - E_J\hat{\phi}^4/24 + \mathcal{O}(\hat{\phi}^6)$. The leading term is quadratic and therefore the Hamiltonian can be described as a QHO with a quartic perturbation. Using ladder operators, the operators $\hat{n}$ and $\hat{\phi}$ are expressed as:

$$\hat{n} = \frac{-i}{2}\left(\frac{E_J}{2E_C}\right)^{1/4}(\hat{a}_- - \hat{a}_+) \quad \text{and} \quad \hat{\phi} = \left(\frac{2E_C}{E_J}\right)^{1/4}(\hat{a}_- + \hat{a}_+) \tag{25}$$

Thus the Hamiltonian of the perturbed QHO in second quantization becomes:

$$\hat{H} = \sqrt{8E_C E_J}(\hat{a}_+\hat{a}_- + 1/2) - E_J - \frac{E_C}{12}(\hat{a}_- + \hat{a}_+)^4 \tag{26}$$

We discard the constant term $-E_J$, yielding a Hamiltonian of the form: $\hat{H} = \hat{H^0} + \lambda\hat{H'}$, where $\hat{H}^0$ represents the unperturbed QHO, and $\hat{H}'$ is the small quartic perturbation. The perturbation parameter $\lambda = \frac{E_C}{12}$ is small compared to $\sqrt{8E_C E_J}$, justifying the treatment of the Hamiltonian as perturbed. From this, the Josephson plasma frequency can be extracted. Notice that n_{offset} can be eliminated by a gauge transformation. The first-order correction to the eigenenergies due to the perturbation is given by:

$$E_j^{(1)} = -\frac{E_C}{12}\langle j^0|(\hat{a}_- + \hat{a}_+|j^0)^4\rangle = -\frac{E_C}{12}(6j^2 + 6j + 3) \tag{27}$$

where j^0 denotes the jth unperturbed state of the QHO. Combining this result with Eq. 20. The anharmonicity in the $(E_J/E_C)^{-1} \ll 1$ limit is found to be: $\alpha = -E_C$. [7, 3]

Flux Tunable Transmon

Both the charging energy and the Josephson energy are determined by the topological design of the qubit. For quantum operations it can be useful to use qubits, which you can tune, while the experiment is in progress. Such a qubit can be constructed using a superconducting quantum interference device

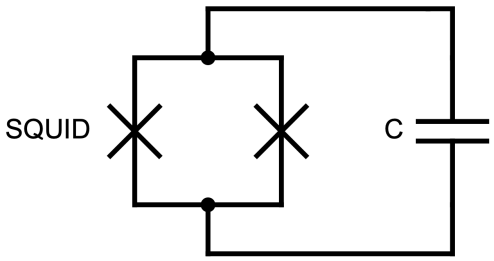

Figure 3: Lumped-element model of a circuit consisting of a capacitor and a SQUID loop

(SQUID). A SQUID can be constructed by placing two Josephson junctions in parallel within the circuit. A flux tunable transmon is therefore a circuit consisting of a capacitor and a SQUID loop (see Fig. 3). The Hamiltonian is given by:

$$\hat{H} = 4E_C(\hat{n} + n_{\text{offset}})^2 - E_{J_L}\cos(\hat{\phi}_L) - E_{J_R}\cos(\hat{\phi}_R) \tag{28}$$

Here, E_{J_L} and E_{J_R} are the Josephson energies for the right and left junction, respectively, while ϕ_L and ϕ_R denote the phase differences across each junction.

Considering a symmetric loop where the Josephson energies for each junction are equal, $E_{J_L} = E_{J_R} = E_J$. We can apply an external magnetic field through the SQUID loop, this will result in an external flux. The flux will distribute itself equally in the symmetric circuit. Resultning in the following Hamiltonian:

$$\hat{H} = 4E_C(\hat{n} + n_{\text{offset}})^2 - E_J\cos(\hat{\phi}_L + \frac{\phi_{ext}}{2}) - E_J\cos(\hat{\phi}_R + \frac{\phi_{ext}}{2}) \tag{29}$$

Where $\phi_{ext} = 2\pi\Phi_{ext}/\Phi_o$. Φ_{ext} is the external flux in units of the magnetic flux quantum. Due to the flux quantization condition. The total flux in the system must obey:

$$\phi_L - \phi_R + \phi_{ext} = 2\pi k \tag{30}$$

Combining Eq. 29 and Eq. 30, and using the fact that the absolute values of the phase differences across the junctions must be equal in the symmetric circuit, $\phi_L = -\phi_R = \phi$, along with the trigonometric identity $2\cos(A)\cos(B) = \cos(A+B) + \cos(A-B)$, we obtain the following Hamiltonian for the flux-tunable transmon:

$$\hat{H} = 4E_C(\hat{n} + n_{offset})^2 - 2E_J\cos(\frac{\phi_{ext}}{2})\cos(\hat{\phi}) \tag{31}$$

Notice that when you define the effective Josephson energy as $E'_J = 2E_J\cos(\phi_{ext}/2)$, you obtain the Hamiltonian for a JC qubit (Eq. 28), where the effective Josephson energy becomes a free parameter. [11, 9]

IV. Numerical Implementation

While it is possible to solve the Hamiltonian for the CPB/transmon and the flux-tunable transmon analytically, it is often simpler and more practical to approach the problem numerically. This section introduces the methods and considerations involved in the numerical implementation.

The initial step of numerical treatment is the choice of basis for representing the quantum states and operators. The flux and charge bases, which are related by a Fourier-like transformation, act as the foundational structure for building the Hamiltonian.

$$|\phi\rangle = \sum_{n=-\infty}^{\infty} e^{in\phi} |n\rangle \quad \text{and} \quad |n\rangle = \frac{1}{2\pi} \int_0^{2\pi} d\phi e^{-in\phi} |\phi\rangle \tag{32}$$

Once the basis choice is made, the flux and charge operator that appear in the Hamiltonian can be expressed as numerical matrices and implemented on the computer. [11]

Operator Representation in the Flux Basis

The reduced variables, $\hat{n}$ and $\hat{\phi}$, are quantum conjugate variables, satisfying the canonical commutation relation $[\hat{\phi}, \hat{n}] = i$. From this, we identify the charge operator as $\hat{n} = -i\frac{\partial}{\partial\hat{\phi}}$. Consequently, the Hamiltonian for the JC circuit (Eq. 23), can now be expressed simply in terms of the phase variable ϕ (n_{offset} is eliminated by a gauge transformation).

$$\hat{H} = -4E_C \frac{\partial^2}{\partial\hat{\phi}^2} - E_J \cos(\hat{\phi}) \tag{33}$$

To numerically implement the Hamiltonian (Eq. 33), we discretize the phase variable ϕ on a finite grid, enabling us to represent the operators in matrix form.

The finite difference approximation, derived from Taylor expansion, is used to discretize the capacitance energy term.

$$f''(x) = \frac{f(x + \Delta x) - 2f(x) + f(x - \Delta x)}{\Delta x^2} \tag{34}$$

The second derivative can, when discretized with central difference approximation, be represented as a tridiagonal matrix. With the diagonal elements being -2 and the off-diagonal elements being 1.

$$\frac{\partial^2}{\partial\hat{\phi}^2} \to \frac{1}{2} \begin{pmatrix} -2 & 1 & 0 & \cdots & 0 \\ 1 & -2 & 1 & \cdots & 0 \\ 0 & 1 & -2 & & \\ \vdots & \vdots & \ddots & \ddots & \vdots \\ 0 & 0 & \cdots & 1 & -2 \end{pmatrix} \tag{35}$$

The inductive energy term does not involve derivatives. In the flux basis, the reduced flux operator, $\hat{\phi}$, is diagonal. Consequently, functions of $\hat{\phi}$, such as $\cos(\hat{\phi})$, are also diagonal in this basis. The diagonal elements of the potential matrix are simply the values of $\cos(\phi_k)$ at the discretized points ϕ_k, with $k = 0, 1, \ldots, N-1$.

$$\cos(\hat{\phi}) \to \begin{pmatrix} \cos(\phi_0) & 0 & \cdots & 0 \\ 0 & \cos(\phi_1) & \cdots & 0 \\ \vdots & \vdots & \ddots & \vdots \\ 0 & 0 & \cdots & \cos(\phi_{N-1}) \end{pmatrix}. \tag{36}$$

[8, 6]

Operator Representation in the Charge Basis

The charge basis is the eigenbasis of the reduced charge operator, because of this its matrix representation is diagonal. To truncate the Hilbert space to a finite size a cutoff parameter, n_{cutoff}, is introduced.

$$\hat{n} \to \begin{pmatrix} -n_{\text{cutoff}} + n_{\text{offset}} & 0 & \cdots & 0 & 0 \\ 0 & -n_{\text{cutoff}} + n_{\text{offset}} + 1 & \cdots & 0 & 0 \\ \vdots & \vdots & \ddots & \vdots & \vdots \\ 0 & 0 & \cdots & n_{\text{cutoff}} + n_{\text{offset}} - 1 & 0 \\ 0 & 0 & \cdots & 0 & n_{\text{cutoff}} + n_{\text{offset}} \end{pmatrix} \tag{37}$$

To express the inductive term operator as a matrix in the charge basis, it is useful to refer back to the basis definition (Eq. 32). The objective is to represent $\cos(\hat{\phi})$ in the charge basis. To achieve this, we apply the operators $e^{\pm i\hat{\phi}}$ to the state $|n\rangle$.

$$e^{\pm i\hat{\phi}} |n\rangle = \frac{1}{2\pi} \int_0^{2\pi} d\phi e^{-in\phi} e^{\pm i\hat{\phi}} |\phi\rangle \tag{38}$$

When expanding the operator for small ϕ we obtain the following approximation: $e^{\pm i\hat{\phi}} \approx \pm(\mathbb{1} + i\hat{\phi} - \frac{1}{2}\hat{\phi}^2 - \frac{i}{6}\hat{\phi}^3 + \ldots)$. Now, consider the eigenvalue equation in the exponent. By solving this and compressing the function back to its exponential form, we find:

$$e^{\pm i\hat{\phi}} = \frac{1}{2\pi} \int_0^{2\pi} d\phi e^{-in\phi} (\pm\mathbb{1} \pm i\hat{\phi}) |\phi\rangle \tag{39}$$

$$= \frac{1}{2\pi} \int_0^{2\pi} d\phi e^{-in\phi} (\pm\mathbb{1} \pm i\phi) |\phi\rangle \tag{40}$$

$$= \frac{1}{2\pi} \int_0^{2\pi} d\phi e^{-i\phi(n\mp 1))|\phi\rangle} \tag{41}$$

This shows that $e^{\pm i\hat{\phi}}$ takes the state from $|n\rangle$ to $|n \mp 1\rangle$. Therefore, the operator can be expressed in Dirac notation as:

$$e^{i\hat{\phi}} = \sum_n |n\rangle \langle n+1| \quad \text{and} \quad e^{-i\hat{\phi}} = \sum_n |n\rangle \langle n-1| \tag{42}$$

The cosine function can be written in terms of exponential operators as $\cos(\hat{\phi}) = \frac{1}{2}\left(e^{i\hat{\phi}} + e^{-i\hat{\phi}}\right)$. Using Eq. 42, we can construct the matrix representation for the operator $\cos(\hat{\phi})$:

$$\cos(\hat{\phi}) \to \frac{1}{2}\begin{pmatrix} 0 & 1 & 0 & \cdots & 0 \\ 1 & 0 & 1 & \cdots & 0 \\ 0 & 1 & 0 & \cdots & 0 \\ \vdots & \vdots & \vdots & \ddots & \vdots \\ 0 & 0 & \cdots & 1 & 0 \end{pmatrix}. \tag{43}$$

Notice that the $\cos(\hat{\phi})$ operator is not limited by any n_{cutoff}. In the numerical implementation, the operator matrices must have the same dimensions. [2, 11]

Computational Framework with QuTip

Now that we have the matrix representation of the operators in the different bases, the building blocks for the numerical implementation are in place. For the simulations, I will use QuTip, an open-source software for simulating the dynamics of quantum systems. Essentially, I will use QuTip as an eigenvalue solver.

V. Simulations

The Cutoff Parameter

Numerical accuracy is an essential consideration when using simulations to forecast measurements. Error analysis in numerical simulations is a complex field, and while a thorough exploration lies beyond the scope of this thesis, this section outlines the approach used to construct the simulations herein. Specifically, we focus on the role of the cutoff parameter, which determines the dimensions of the Hilbert space. N is the cutoff parameter in the flux basis and n_{cutoff} is the cutoff parameter in the charge basis. Choosing an appropriate value for the cutoff parameter requires balancing two factors: (1) ensuring that the simulation achieves sufficient accuracy for its intended purpose, and (2) avoiding excessive computational operations. In the context of the transmon qubit, selecting a cutoff parameter that is too small leads to inaccurate results: eigenenergies become

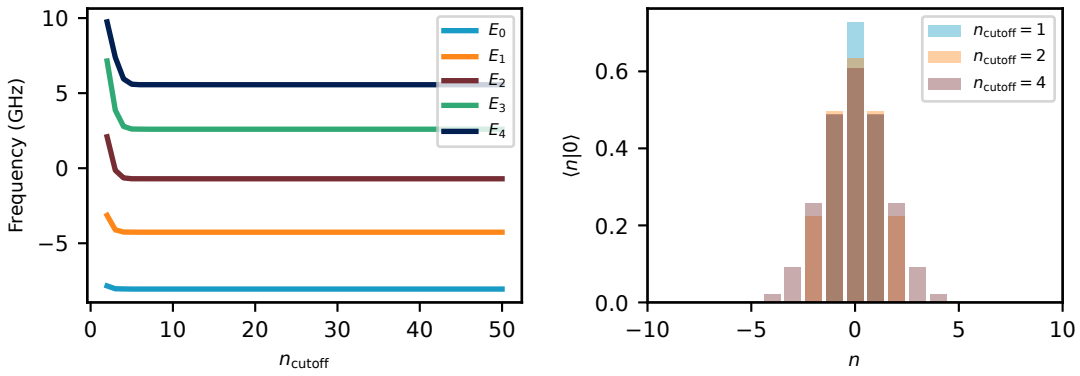

(a) **(b)**

Figure 4: Both simulations are performed in the transmon regime, $E_J/E_C = 50$, with $E_C = 0.2\,\text{GHz}$. **(a)** The first five eigenenergies as a function of n_{cutoff}, demonstrating how truncating the charge basis too severely leads to significant deviations in the computed eigenenergies. **(b)** The ground state overlaps $\langle n|0\rangle$ in the charge basis, showing the real part of the overlaps $\text{Re}(\langle n|0\rangle)$ as a function of charge states n for different cutoff parameter values n_{cutoff}. The results illustrate the importance of a sufficiently large Hilbert space to accurately capture both the eigenenergies and the ground state wavefunction in the charge basis.

too large, and wave functions are excessively narrow, as illustrated in Fig. 4. To gain an intuitive understanding for these effects, it is useful to consider the QHO. Recall that the potential energy of a QHO is $V(x) = \frac{1}{2}m\omega^2x^2$. The angular frequency, ω, determines how quickly the potential grows as x moves away from $x = 0$. When the angular frequency is large, the potential becomes steeper, meaning it grows more rapidly with x. This results in the width of the potential becoming narrow. When the angular frequency is small the potential grows more slowly with x, i.e. the width of the potential is larger.

The ground state of the QHO is a Gaussian distribution, $\psi_0 = (\frac{m\omega}{\pi\hbar})^{\frac{1}{4}}e^{-\frac{m\omega}{\pi\hbar}x^2}$. The width of the ground state is inversely proportional to $\sqrt{\omega}$. Like the potential, the larger the angular frequency, the narrower the ground state. It is not surprising that the width of the potential and the width of the ground state correspond, as the wavefunction is constrained by the potential it is bound to.

The ground state energy of the QHO is proportional to the angular frequency, $E_0 = \frac{1}{2}\hbar\omega$. It can thus be concluded for the case of the QHO that a wider potential results in lower ground state energies.

This picture can be used to understand why the eigenenergies of the transmon initially decrease as the cutoff parameter increases in Fig. 7a. Expanding the potential of the

transmon for small ϕ, we see that the leading terms is quadratic, and thus the potential of the transmon behaves like the potential of the QHO. Therefore, when compressing the wavefunction, by picking too small of a cutoff parameter, the potential becomes steeper and the eigenenergies larger.

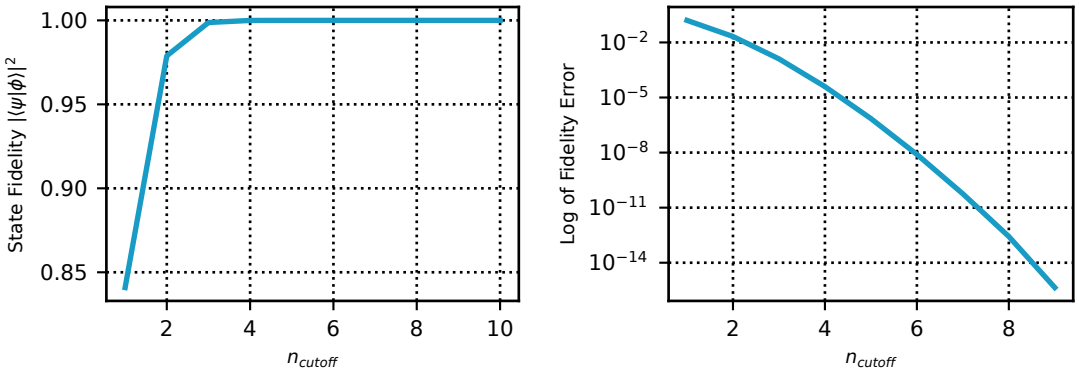

(a) **(b)**

Figure 5: Both simulations are conducted in the transmon regime with $E_J/E_C = 50$ and $E_C = 0.2$ GHz. **(a)** State fidelity between the ground state of a transmon with a large cutoff value ($n_{\text{cutoff}} = 10$) and the ground states calculated for smaller cutoff values. As n_{cutoff} increases, the fidelity approaches 1, signifying perfect overlap with the target ground state. **(b)** Log of the fidelity error, which exhibits a nearly linear trend, indicating that the fidelity grows approximately exponentially with n_{cutoff} until it converges to 1, signifying a perfect overlap.

A technique to determine an appropriate cutoff value is to consider the state fidelity. The state fidelity is a measure of how closely a quantum state produced by a system matches a desired target state. It quantifies the overlap between the two states, with a fidelity of 1 indicating perfect overlap and 0 indicating no overlap at all. The state fidelity of a pure state $|\psi\rangle$ and a target state $|\phi\rangle$ is given by:

$$\mathcal{F}(|\psi\rangle, |\phi\rangle) = |\langle\psi|\phi\rangle|^2 \tag{44}$$

Fig. 5 presents a simulation of the state fidelity as a function of the cutoff parameter for the transmon example. This simulation is meant to demonstrate that the state fidelity increases almost exponentially, until it reaches 1, where it remains constant. Computational efficiency was not a consideration for this simulation. However, when working with large systems, state fidelity can serve as an effective measure for determining the cutoff parameter. By calculating the target state once, which may require significant computational power, you create a reference state for comparison.

Charge Noise Sensitivity

As previously discussed, the energy ratio E_J/E_C plays a significant role in the properties of qubits constructed from JC circuits. The transmon is particularly notable because, unlike the CPB, it is unaffected by charge noise.

Fig. 6 illustrates how the width of the wavefunction in the charge basis increases as the E_J/E_C ratio increases, meaning the wavefunction becoming increasingly delocalized. Thus, the probability of having a larger difference in Cooper pairs between the two islands increases with the energy ratio. This suggests that a widely spread wave function is less sensitive to charge noise from the surroundings. In contrast, for a CPB, even a small enviromental charge offset can significantly affect the system.

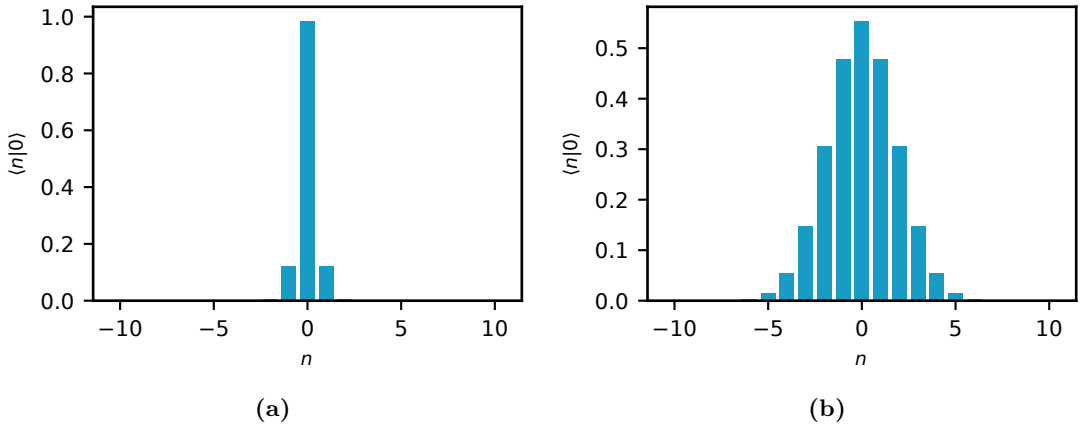

Figure 6: Ground state overlaps $\langle n|0\rangle$ in the charge basis for three qubits constructed from JC circuits, characterized by different E_J/E_C-ratios. All systems have $E_C = 0.2$ GHz, with different values of E_J. **(a)** The CPB regime, $E_J = E_C$, shows a strongly localized wavefunction in the charge basis. **(b)** The extreme transmon regime, $E_J = 100E_C$, exhibits a delocalized wavefunction indicative of reduced sensitivity to charge noise. The cutoff parameter is set to $n_{\text{cutoff}} = 10$ for all cases.

Anharmonicity

Increasing the E_J/E_C ratio comes at the cost of reducing the qubit's anharmonicity. This relationship is visualized in Fig. 8a. For small values of E_J/E_C, the system exhibits significant anharmonicity, characteristic of the CPB regime. As E_J/E_C increases, the anharmonicity decreases, reflecting the transition to the transmon regime. For large energy ratios, the anharmonicity asymptotically approaches $-E_C$. [7]

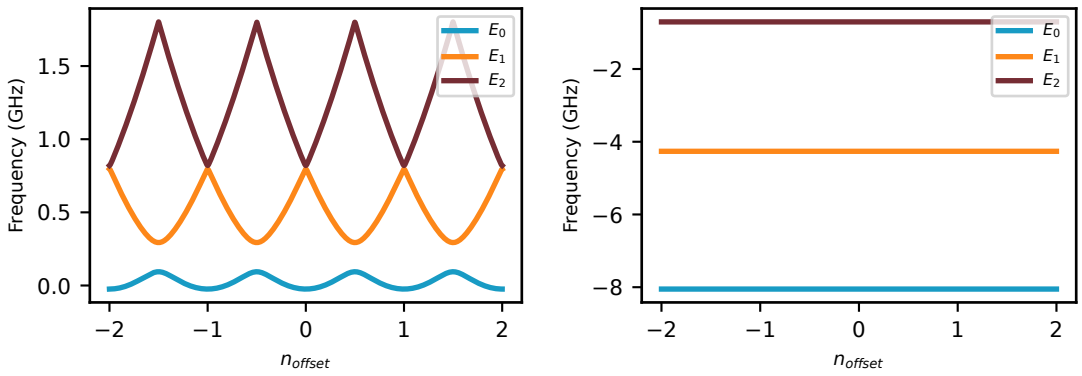

(a) **(b)**

Figure 7: Charge dispersion of the first three eigenenergies E_0, E_1, and E_2 as a function of offset charge n_{offset}. **a)** For a CPB with $E_C = 0.2$ GHz and $E_J = E_C$, the eigenenergies exhibit a strong charge noise sensitivity. **b)** For a transmon with $E_C = 0.2$ GHz and $E_J = 50E_C$, the eigenenergies are nearly independent of fluctiations in n_{offset}, illustrating the charge insensitivity of the transmon regime. Both simulations use $n_{\text{cutoff}} = 10$.

Comparing the Potential of JC and LC Circuits

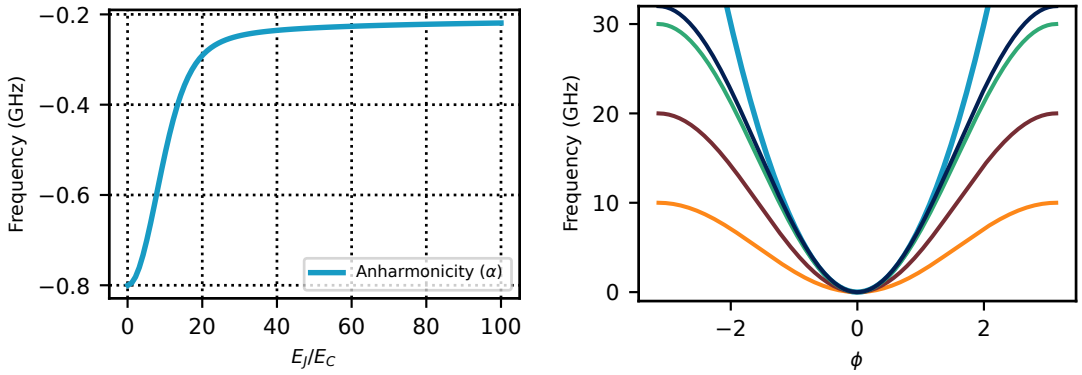

(a) **(b)**

Figure 8: **(a)** Anharmonicity α as a function of the energy ratio E_J/E_C in the charge basis. The absolute value of the anharmonicity decreases until it asymptotically approaches $-E_C$. The simulation uses a cutoff value of $n_{\text{cutoff}} = 10$, with $E_C = 0.2$ GHz. **(b)** Potential energy profiles for the LC and JC circuits in the flux basis. The potentials are shifted such that their minimum values are set to 0 for comparison. For all cases, $E_C = 0.2$ GHz and $E_L = 75E_C$. As E_J increases, the anharmonic potential of the JC circuit gradually approaches the harmonic potential of the LC circuit. The plotted potentials correspond to E_J values of $25E_C$, $50E_C$, $75E_C$, and $80E_C$, illustrating how the JC circuit potential becomes increasingly harmonic with larger E_J.

A helpful way to understand why the size of the anharmonicity decreases as a function

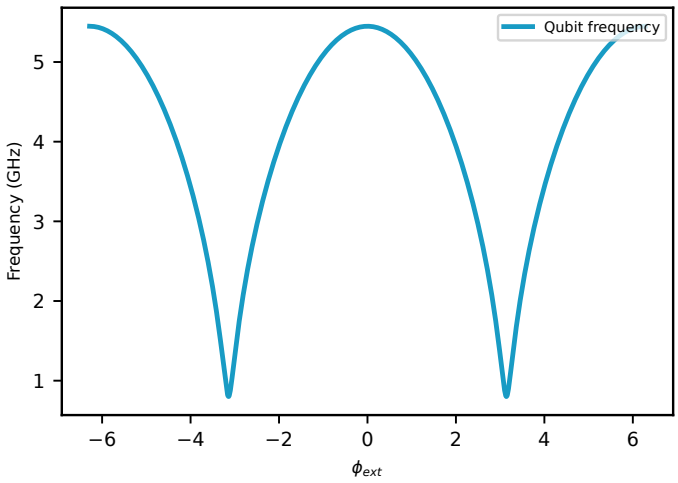

Figure 9: Qubit frequency as a function of the reduced external flux ϕ_e for a flux-tunable transmon. The calculations are performed for $E_J = 50E_C$, with $E_C = 0.2$ GHz and $n_{\text{cutoff}} = 10$.

of the energy ratio is by, once again, recall the QHO, which has equidistant energy-level spacing, i.e an anharmonicity which equals zero. Comparing the potential of a QHO with that of the JC circuit for different E_J/E_C ratios. As the ratio increases, the potential of the JC circuit increasingly resembles a quadratic potential, similar to that of the QHO. (see Fig. 8b). Since the anharmonicity is governed by the potential, it is intuitive that the anharmonicity of the JC circuit decreases as the potential becomes more harmonic. At sufficiently high E_J/E_C ratios, where E_J essentially sets the amplitude of the cosine potential, the potential of the transmon becomes exceedingly narrow. In this regime, the anharmonicity approaches $-E_C$, and the first few energy levels become strongly localized within the potential well, forming bound states.

Flux-Tunable Transmon

The anharmonicity of the JC circuit, as explored in the previous section, depends strongly on the ratio E_J/E_C, with larger E_J values causing the potential to become more harmonic. In the flux-tunable transmon, the effective Josephson energy, $E'_J = -E_J \cos(\phi_{\text{ext}}/2)$, can be controlled by adjusting the external flux ϕ_{ext}. This allows access to the qubit during an experiment and enables operations such as bringing two qubits into resonance, a feature that is useful for certain qubit operations. By tuning the external flux, the amplitude of the cosine potential is modified, effectively adjusting the anharmonicity of the system. Fig. 9 presents the qubit frequency of a flux-tunable transmon as a function of the external flux, showing complete destructive interference at $\Phi_{\text{ext}} = \frac{1}{2}\Phi_0$.

VI. Conclusion and Outlook

Conclusion

The primary goal of this thesis was to provide a comprehensive introduction to superconducting circuits, starting with the quantum harmonic oscillator (QHO), which played a significant role throughout the thesis. A substantial part of this work was dedicated to exploring the influence of the E_J/E_C ratio on qubit properties. By conducting simulations, I gained valuable insights into the physical properties of superconducting circuits, particularly the relationship between charge sensitivity and anharmonicity. The simulations confirmed the theoretical expectations, such as the importance of the cut-off parameter in ensuring accurate eigenenergies and ground state wavefunctions. For instance, truncating the charge basis too severely can lead to significant deviations in the calculated eigenenergies. Additionally, simulating wavefunctions in different E_J/E_C regimes showed how the delocalization of the wavefunction is connected to the qubit's sensitivity to charge noise. In the CPB regime, the wavefunction is strongly localized, while in the transmon regime, the wavefunction becomes increasingly delocalized, reflecting reduced sensitivity to charge noise. The anharmonicity of the JC qubit was also examined, and the simulations confirmed the expected trend, where the absolute value of the anharmonicity decreases as the E_J/E_C ratio increases, approaching $-E_C$ as E_J becomes large. The potential profiles of the LC and JC circuits further illustrated how the anharmonic potential of the JC circuit gradually approaches the harmonic potential of the LC circuit as E_J increases. Lastly, the flux-tunable transmon was investigated, demonstrating the ability to control the qubit by adjusting the external flux, emphasizing its advantages for qubit control in quantum computation.

Outlook

Looking ahead, an area of interest I would love to explore further is the topological design and fabrication process of qubits. This includes understanding how E_J and E_C arise from the physical layout of the qubit, as well as delving into the intricate fabrication techniques involved. While this thesis has focused on the physical properties of superconducting qubits, exploring qubit manipulation and decoherence would be a natural next step in my research journey.

Acknowledgments

I would like to thank Morten Kjaergaard for opening his lab to me and providing the opportunity to write my thesis under his guidance. I greatly appreciate his mentorship

and the insightful discussions we had throughout this process. A special thanks to everyone in the SQUID lab for their warm and welcoming atmosphere. During my time there, I truly felt like a part of the team. I had the chance to engage in group meetings, journal clubs, and attend inspiring talks. I also gained hands-on experience with the two new XLDsl dilution refrigerators. I would like to extend my gratitude to Casper Wied for reading my thesis and providing valuable feedback. I also want to thank my office mates in the master's office, especially Leo Uhre Jakobsen, for his insightful discussions and contributions to my theoretical understanding, and Rune Kutchinsky for his help with the layout. Finally, I would like to thank Rasmus Bo Nielsen for proof-reading my work.

References

[1] James F. Annett. *Superconductivity, Superfluids and Condensates*. Oxford University Press, 2004.

[2] Philipp Aumann et al. "CircuitQ: an open-source toolbox for superconducting circuits". In: *New Journal of Physics* 24.9 (Sept. 2022), p. 093012. ISSN: 1367-2630. DOI: 10.1088/1367-2630/ac8cab. URL: http://dx.doi.org/10.1088/1367-2630/ac8cab.

[3] Darrell F. Schroeter David J. Griffiths. *Introduction to Quantum Mechanics, third edition*. Cambridge University Press, 2018.

[4] Nicolas Gisin et al. "Quantum cryptography". In: *Reviews of Modern Physics* 74.1 (Mar. 2002), pp. 145–195. ISSN: 1539-0756. DOI: 10.1103/revmodphys.74.145. URL: http://dx.doi.org/10.1103/RevModPhys.74.145.

[5] Goldstein et al. *Classical mechanics*. Pearson, 2014.

[6] M.T. Heath. *Scientific Computing: An Introductory Survey*. McGraw-Hill Education, 2005. ISBN: 9780071244893. URL: http://books.google.de/books?id=gwBrMAEACAAJ.

[7] Jens Koch et al. "Charge-insensitive qubit design derived from the Cooper pair box". In: *Physical Review A* 76.4 (Oct. 2007). ISSN: 1094-1622. DOI: 10.1103/physreva.76.042319. URL: http://dx.doi.org/10.1103/PhysRevA.76.042319.

[8] Anton Frisk Kockum and Franco Nori. "Quantum Bits with Josephson Junctions". In: *Fundamentals and Frontiers of the Josephson Effect*. Springer International Publishing, 2019, pp. 703–741. ISBN: 9783030207267. DOI: 10.1007/978-3-030-20726-7_17. URL: http://dx.doi.org/10.1007/978-3-030-20726-7_17.

[9] P. Krantz et al. “A quantum engineer’s guide to superconducting qubits”. In: *Applied Physics Reviews* 6.2 (June 2019). ISSN: 1931-9401. DOI: 10.1063/1.5089550. URL: http://dx.doi.org/10.1063/1.5089550.

[10] Y. Nakamura, Yu. A. Pashkin, and J. S. Tsai. “Coherent control of macroscopic quantum states in a single-Cooper-pair box”. In: *Nature* 398.6730 (Apr. 1999), pp. 786–788. ISSN: 1476-4687. DOI: 10.1038/19718. URL: http://dx.doi.org/10.1038/19718.

[11] S.E. Rasmussen et al. “Superconducting Circuit Companion—an Introduction with Worked Examples”. In: *PRX Quantum* 2.4 (Dec. 2021). ISSN: 2691-3399. DOI: 10.1103/prxquantum.2.040204. URL: http://dx.doi.org/10.1103/PRXQuantum.2.040204.

[12] Peter W. Shor. “Polynomial-Time Algorithms for Prime Factorization and Discrete Logarithms on a Quantum Computer”. In: *SIAM Journal on Computing* 26.5 (Oct. 1997), pp. 1484–1509. ISSN: 1095-7111. DOI: 10.1137/s0097539795293172. URL: http://dx.doi.org/10.1137/S0097539795293172.

[13] Uri Vool and Michel Devoret. “Introduction to quantum electromagnetic circuits”. In: *International Journal of Circuit Theory and Applications* 45.7 (June 2017), pp. 897–934. ISSN: 1097-007X. DOI: 10.1002/cta.2359. URL: http://dx.doi.org/10.1002/cta.2359.

Appendices

A: Full Derivation of the Hamiltonian for the LC Circuit in the Flux Basis

In this derivation, the circuit elements are described in the flux basis. The flux, $\Phi(t)$, is defined as a time integral of the voltage:

$$\Phi(t) = \int_{-\infty}^{t} V(t')dt' \Rightarrow V = \dot{\Phi}$$

Consequently, the flux is position-like, while the charge is momentum-like. The instantaneous, time dependent energy of the circuit elements is expressed as:

$$E(t) = \int_{-\infty}^{t} V(t')I(t')dt'$$

The current can be rewritten in terms of capacitance:

$$I = C\frac{dV}{dt} = C\ddot{\Phi}$$

The kinetic energy corresponding to the capacitor is then:

$$\mathcal{T}_C = \int_{-\infty}^{t} C\dot{\Phi}\ddot{\Phi}dt'$$

Using $\frac{d}{dt}(\frac{1}{2}\dot{\Phi}^2) = \dot{\Phi}\ddot{\Phi}$ and applying the Fundamental Thereom of Calculus, we obtain:

$$\mathcal{T}_C = \frac{C}{2}\dot{\Phi}^2$$

Similarly, the current can be expressed using the inductance:

$$V = L\frac{dI}{dt} = \dot{\Phi} \Rightarrow I = \frac{\Phi}{L}$$

The potential energy, corresponding to the inductor, is calculated analogously:

$$\mathcal{U}_L = \int_{-\infty}^{t} \frac{1}{L}\Phi\dot{\Phi} = \frac{1}{2L}\Phi^2$$

The Lagrangian of the system is given by:

$$\mathcal{L} = \frac{C}{2}\dot{\Phi}^2 - \frac{1}{2L}\Phi^2$$

The canonical momentum is defined as:

$$Q = \frac{\partial \mathcal{L}}{\partial \dot{\Phi}} = C\dot{\Phi}$$

The Hamiltonian is obtained via the Legendre transformation:

$$H = Q\dot{\Phi} - \mathcal{L} = \frac{Q^2}{2C} + \frac{\Phi^2}{2L}$$

In terms of voltage and current, this is equivalent to

$$H = \frac{1}{2}CV^2 + \frac{1}{2}LI^2$$

B: Full Derivation of the Hamiltonian for LC Circuit in the Charge Basis

As mentioned the Hamiltonian can also be derived using the charge as the generalized coordinate to describe the circuit elements. In this basis, the charge, Q, is position-like, and the flux Φ, is momentum-like. Consequently, the magnetic energy of the inductor becomes the kinetic energy, while the electric energy of the capacitor represents the potential energy. The charge is defined as the time integral of the current

$$Q(t) = \int_{-\infty}^{t} I(t')dt' \Rightarrow I = \dot{Q}$$

The voltage, in terms of inductance, is expressed as:

$$V = L\frac{dI}{dt} \Rightarrow V = L\ddot{Q}$$

The kinetic energy, corresponding to the inductor, is:

$$\mathcal{T}_L = \int_{-\infty}^{t} L\ddot{Q}\dot{Q}dt'$$

Using $\frac{1}{2}\frac{d}{dt}(\dot{Q}^2) = \ddot{Q}\dot{Q}$ as well as the Fundamental Thereom of Calculus, we obtain:

$$\mathcal{T}_L = \frac{L}{2}\dot{Q}^2$$

The relationship between the voltage and the capacitance is given by:

$$I = C\frac{dV}{dt} = \dot{Q} \Rightarrow V = \frac{Q}{C}$$

The potential energy across the capacitor is therefore:

$$\mathcal{U}_C = \int_{-\infty}^{t} \frac{Q}{C}\dot{Q}dt'$$

Similar to the kinetic energy calculation, applying the product rule and the Fundamental Theorem of Calculus yields:

$$\mathcal{U}_C = \frac{1}{2C}Q^2$$

The Lagrangian is defined as the difference between the kinetic energy and the potential energy:

$$\mathcal{L} = \mathcal{T}_L - \mathcal{U}_C = \frac{L}{2}\dot{Q}^2 - \frac{1}{2C}Q^2$$

The canonical momentum is:

$$\Phi = \frac{d\mathcal{L}}{d\dot{Q}} = L\dot{Q}$$

The Hamiltonian is obtained through the Legendre transformation:

$$H = \Phi\dot{Q} - \mathcal{L} = \frac{1}{2L}\Phi^2 + \frac{1}{2C}Q^2$$

In terms of voltage and current, this is equivalent to

$$H = \frac{1}{2}LI^2 + \frac{1}{2}CV^2$$

C: The Canonical Commutation Relation Between $\hat{x}$ and $\hat{p}$

Using $\hat{p} = -i\hbar\frac{d}{dx}$ as well as a test function, $f(x)$.

$$\begin{aligned}
[\hat{x},\hat{p}]f(x) &= (x(-i\hbar)\frac{d}{dx}(f(x)) - (-i\hbar)\frac{d}{dx}(xf(x))) \\
&= -i\hbar(x\frac{d}{dx}(f(x)) - x\frac{d}{dx}(f(x)) - f(x)) \\
&= i\hbar f(x) \\
&\Rightarrow [\hat{x},\hat{p}] = i\hbar
\end{aligned}$$

D: Deriving the Ground State and the Ground State Energy of the QHO

$$\begin{aligned}
&\hat{a}_- = 0 \\
\Rightarrow &\frac{1}{\sqrt{2\hbar m\omega}}(i\hbar\frac{d}{dx} + m\omega x)\psi_0 = 0 \\
\Rightarrow &\frac{d\psi_0}{dx} = -\frac{m\omega}{\hbar}x\psi_0
\end{aligned}$$

Using seperation of variables:

$$\int \frac{d\psi_0}{\psi_0} = -\frac{-m\omega}{\hbar}\int x dx \Rightarrow \ln\psi_0 = -\frac{m\omega}{2\hbar}x^2 + \text{constant}$$
$$\Rightarrow \psi_0 = Ae^{\frac{-m\omega}{2\hbar}x^2}$$

To normalize:

$$\begin{aligned}
\int_{-\infty}^{\infty} |\psi_0(x)|^2 dx &= 1 \\
\int_{-\infty}^{\infty} A^2 e^{-\frac{m\omega}{\hbar}x^2} dx &= 1 \\
A^2\sqrt{\frac{\pi\hbar}{m\omega}} &= 1 \\
\Rightarrow A &= \left(\frac{m\omega}{\pi\hbar}\right)^{1/4}
\end{aligned}$$

Thus, the normalized ground state wavefunction is:

$$\psi_0(x) = \left(\frac{m\omega}{\pi\hbar}\right)^{1/4} e^{-\frac{m\omega}{2\hbar}x^2}$$

The Hamiltonian of the QHO can be expressed as:

$$\hat{H} = \hbar\omega \left(\hat{a}_+ \hat{a}_- + \frac{1}{2} \right)$$

The number operator $\hat{a}_+ \hat{a}_-$ has eigenvalues $n = 0, 1, 2, \ldots$, corresponding to the quantum number for the energy levels of the harmonic oscillator.
The ground state energy corresponds to the lowest eigenvalue of the number operator, which is $n = 0$. Thus, the ground state energy is:

$$E_0 = \frac{1}{2}\hbar\omega$$